Absorption and Zeeman effect in Nd^{3+}-doped $LiYF_4$: measurements and simulation

1996 J. Phys.: Condens. Matter 8 4643

(http://iopscience.iop.org/0953-8984/8/25/019)

J. Phys.: Condens. Matter **8** (1996) 4643–4659. Printed in the UK

Absorption and Zeeman effect in Nd^{3+}-doped $LiYF_4$: measurements and simulation

M A Couto dos Santos†, P Porcher†, J C Krupa‡ and J Y Gesland§

† Laboratoire de Chimie Métallurgique et Spectroscopie des Terres Rares, UPR 209, CNRS, 1 place A Briand, 92125 Meudon, France

‡ Laboratoire de Radiochimie, IPN, BP1, 91406 Orsay, France

§ Groupe de Cristallogénèse, Université du Maine 72017, Le Mans, France

Received 16 October 1995, in final form 2 February 1996

Abstract. The Nd^{3+} ion energy level scheme in a $LiYF_4$ crystal host is re-examined by absorption spectroscopy and Zeeman measurements. Some other Kramers doublets have been observed. A total of 137 experimental levels has been input in the fitting procedures before the application of the magnetic field. The calculations were performed assuming the approximate D_{2d} rare-earth site symmetry, and the correct S_4, with all parameters varying freely. In both symmetries we have obtained a rms deviation of 17.7 cm^{-1}. In the presence of a magnetic field B, linear and non-linear anticrossing degeneracy lifting, together with negligible Kramers degeneracy lifting, has been observed. In particular, with $B \perp c$, the third component of the $^4G_{7/2}$ level behaves in the former way with a splitting of 22 cm^{-1}, for $B = 6.3$ T, and $^4G_{5/2}$ behaves in the latter way ($B \| c$). It was possible *only* to describe these features all together by introducing the magnetic Hamiltonian $\mu B(L + g_e S)$ in the secular determinant *before diagonalization*. Then, the 364 eigenstates and eigenfunctions of the $4f^3$ configuration are calculated. The isolated doublets in the energy level scheme *and* having a small value of the g-factor, split linearly. In this situation, the framework of perturbation theory was used to obtain satisfactory splitting s-factors. Those not isolated *or* with a large g-factor have a non-linear anticrossing behaviour. The splitting of the lowest component of the $^4I_{9/2}$ ground-state multiplet is observed through a transition which is present in the lowest Zeeman component of the $^4F_{7/2}$ level. This is quite well reproduced by the simulation.

1. Introduction

The application of the trivalent rare-earth(RE)-doped materials for solid state lasers and luminescent devices has led to a large amount of work on these composite media [1–6]. In [4] a review of electroluminescence is given, and [6] consists of a spectral analysis of the RE-doped transparent solids, as well as *a priori* calculations of the crystal-field parameters. The lack of current knowledge on RE materials shows that this kind of study is still important.

The RE-doped lithium yttrium double fluoride is a good crystal host for laser technology. It belongs to the scheelite-type structure, with the $I4_1/a(C_{4h}^6)$ (No. 88) space group, and the RE ions occupy a single crystallographic position with S_4 as point symmetry, very close to D_{2d}. The difference between the two crystallographic point groups is a consequence of the small angular displacement between the two perpendicular tetrahedra formed by the nearest- and next-nearest-neighbour F^- ions (86.3° in the place of 90° [3]). Consequently, the values of the imaginary part of the crystal-field parameters ($k = 4$ and 6) are expected to be small [3, 7].

0953-8984/96/254643+17$19.50

This crystal medium has already been analysed [8, 9]. In particular, the energy levels and the line intensities of this matrix doped with Nd^{3+} ions in the absence of magnetic fields have been simulated by the usual parametrization methods [3, 9, 10]. However, very restrictive conditions have been used in [3] where only the ^4I_J ground-state levels, the first coordination sphere interactions and a T_d crystal-field Hamiltonian are taken into account.

Measurements under a magnetic field of the RE-doped materials have been made by several techniques [11–14]. The magnetic interaction is usually treated in the framework of perturbation theory [15–19]. The aim of this work is to re-examine the spectra of the Nd^{3+}-doped $LiYF_4$ crystal in three parts:

(i) to search in the IR to UV absorption spectrum for the lines not observed until now and then to apply a phenomenological simulation to a more complete scheme of experimental energy levels, assuming both D_{2d} and S_4 site symmetries;

(ii) to perform Zeeman effect measurements in externally applied DC magnetic fields, parallel and perpendicular to the crystallographic axis c;

(iii) to simulate through phenomenological parameters the energy level scheme under a magnetic field by introducing the magnetic operator $L + g_e S$ in the secular determinant *before diagonalization*, since perturbation theory does not describe the non-linear Zeeman effect.

2. Experimental details and measurements

In this work a 1% Nd(III)-doped $LiYF_4$ crystal is studied. The sample has been grown by the Czochralski method [20], cut along the crystallographic axes, polished as a cube with dimensions 5 mm × 5 mm × 5 mm and oriented by the Laue diffractometry technique. The absorption spectra in the absence of a magnetic field were recorded in a Cary 2400 model spectrophotometer, with an average resolution of 0.07 nm, from the near-IR to the near-UV spectral region, 208–2550 nm (48 077–3922 cm^{-1}), with temperatures from 9 to 300 K. The attention is focused on some multiplets ($^4I_{9/2}$, $^4F_{7/2}$, $^4S_{3/2}$, $^4F_{9/2}$, $^4G_{5/2}$ and $^4G_{7/2}$), as well as on transitions not yet observed, for Zeeman effect measurements and simulation purposes. The spectra under a magnetic field were recorded only in the visible region in a Czerny–Turner type HR 1000 Jobin–Yvon monochromator equipped with a R374 Hamamatsu photomultiplier whose resolution is 0.05 nm. A liquid-helium bath cryostat (ASSO, developed in the IPN, Orsay) is used to maintain the temperature at 4.2 K. To establish the DC magnetic fields, superconductor coils of a Nb–Ti alloy are used ($T_C \approx 6$ K), placed in the Helmholtz configuration. This system generates a homogeneous magnetic field within a volume of 1 cm^3, with intensities up to 6.3 T. The values of the magnetic field used here are $B = 0$, 3, 4.6, 5.5 and 6.3 T. Polarization measurements have also been carried out to allow discussion on the irreducible representation of the levels and to define the positions of some lines better.

3. Theoretical background

The general Hamiltonian of an atom or ion in the presence of crystal and magnetic fields can be written as follows:

$$H = H_{FI} + H_{CF} + H_M \tag{1}$$

where the first and second terms are the free-ion and crystal-field contributions, respectively, as indicated below [22]:

$$H_{FI} = H_0 + \sum_{v=0,1,2,3} E^v(nf,nf)e_v + \zeta A_{SO} + \alpha L(L+1) + \beta G(\mathrm{G}_2) + \gamma G(\mathrm{R}_7) + \sum_{\lambda=2,3,4,6,7,8} T^\lambda t_\lambda \tag{2}$$

$$H_{CF} = \sum_{k=2}^{4,6}\sum_{q=0}^{k}[B_q^k(C_q^k + (-1)^q C_{-q}^k) + \mathrm{i}S_q^k(C_q^k - (-1)^q C_{-q}^k)]. \tag{3}$$

H_0 is the spherically symmetric part, E^v are the Racah parameters and e_v is the angular part of the electrostatic repulsion. ζ is the spin–orbit constant and A_{SO} its angular part. α, β and γ are the two-body parameters, L is the total angular momentum operator, and $G(\mathrm{G}_2)$ and $G(\mathrm{R}_7)$ are the Casimir operators. T^λ are the Judd three-body parameters. The t_λ are operators transforming according to the irreducible groups G_2 and R_7. H_{FI} does not include the M^k and P^k integrals correspond to the spin–spin and spin–other orbit magnetic interactions [8, 21]. In the crystal-field Hamiltonian, B_q^k and S_q^k are the real and imaginary parts, respectively, of the crystal-field parameters and C_q^k are the Racah operators associated with the spherical harmonics ($k = 2, 4, 6$). When all these interactions are included, the configuration degeneracy is more or less lifted. For configurations involving an odd number of electrons, all states are Kramers doublets associated with irreducible representations of the double group (Γ_6, Γ_7 for D_{2d} and the pairs Γ_5, Γ_6 and Γ_7, Γ_8 for S_4). In the case of Nd^{3+}-doped $LiYF_4$ the configuration comprises 182 doublets and can be classified in two submatrices by introducing the crystalline quantum number μ, which divides the secular determinant and saves computing time.

The last term of equation (1) is given by

$$H_M = \mu_B B(L + g_e S) \tag{4}$$

which describes the interaction between the crystal and the applied magnetic field B. μ_B is the Bohr magneton, S is the spin operator and g_e is the gyromagnetic spin factor. Although that interaction is almost always considered as a perturbation operating on the crystal-field wavefunctions, we introduce it in the secular determinant *before* diagonalization. This means that a 364-dimensional secular determinant is diagonalized and all quantum states are associated with one-dimensional irreducible representations. The corresponding matrix element can be expressed by

$$H_M = \langle \xi SLJM|L_i + g_e S_i|\xi S'L'J'M'\rangle \tag{5}$$

where i stands for the three components of the $L + g_e S$ tensor of rank 1, $|\xi SLJM_J\rangle$ is the Russell–Saunders basis on which the $4f^N$ configuration states are described, J is the total angular momentum operator, M_J its projection in the z direction and ξ takes into account the other quantum numbers necessary to define unambiguously the quantum states.

Using the Wigner–Eckart theorem, the matrix element in equation (5) turns out to be

$$\langle \xi SLJM|L_i + g_e S_i|\xi' S'L'J'M'\rangle = \delta(\xi,\xi')\delta(S,S')\delta(L,L')(-1)^{J-M} \times \begin{pmatrix} J & 1 & J' \\ -M & i & M' \end{pmatrix} \langle \xi SLJ\|L + g_e S\|\xi SLJ'\rangle. \tag{6}$$

The reduced matrix element on the right-hand side of equation (6) is expressed in terms of the SLJ quantum numbers [23, 24] and the quantum selection rules are given by the 3-j

symbol:

$$H_M = 0 \text{ unless } \begin{cases} -M + i + M' = 0 \\ \Delta(J, J') = 0, \pm 1. \end{cases} \tag{7}$$

The magnetic field removes the Kramers degeneracy by separating the $\pm$ components of M_J. Although the final object of the work is the diagonalization of a secular determinant including the Zeeman effect operator, it is convenient to keep the formalism of the perturbation theory for expressing the experimental data, when the Kramers doublets are well isolated, in the sense that their behaviour is linear versus B. Thus, the energy should be

$$E_M = E^{\pm} = \langle H_M \rangle^{\pm}. \tag{8}$$

The dependence of E_M is linear in M_J for pure states. This is not the case for the RE ions. It is then more appropriate to define the coefficient of the magnetic field as a splitting factor s_i [25], by expressing $E^{\pm}$ as follows:

$$E_i^{\pm} = s_i^{\pm} B \tag{9}$$

where i stands for the parallel and perpendicular orientations of the axis c with respect to B. The general expressions for $s_i^{\pm}$ are

$$s_{\parallel}^{\pm} = \mu_B g_{\parallel} \sum_m a_m^2 M_{J_m} \tag{10}$$

$$s_{\perp}^{\pm} = \mu_B g_{\perp} \sum_m b_m^2 (J_m \mp M_{J_m})(J_m \pm M_{J_m} + 1). \tag{11}$$

a_m and b_m are the coefficients of the linear combination that describes the split $4f^N$ configuration as a function of the states $|\xi S L J M_J\rangle$. $g_{\perp}$ and $g_{\parallel}$ are Landé factors according to the orientation of the c axis with respect to the magnetic field.

The total energy is $E_T^{\pm} = E + E_i^{\pm}$. Then $\Delta E = E_T^{+} - E_T^{-}$ is directly deduced from the curves of the Kramers doublets splitting versus B to obtain s_i as follows:

$$\Delta E = (s_i^{+} - s_i^{-})B = s_i B. \tag{12}$$

The mixing of the RE states and the prevailing non-linear behaviour of ΔE as a function of B make the phenomenological simulation an important tool to reproduce the RE energy level scheme.

4. Results and discussion

4.1. Optical spectra

The spectra recorded without a magnetic field, compared with and eventually completed using the values found in the literature [3] have allowed the identification of 137 of the 182 levels of the Nd^{3+} ion configuration. When transitions overlap, a Gaussian or Lorentzian deconvolution has been used to determine the peak positions precisely.

The following figures show the absorption spectra with and without a magnetic field. The set of multiplets, $^4F_{7/2}$, $^4S_{3/2}$, $^4G_{5/2}$ and $^4G_{7/2}$, is used as example of the general splitting behaviour (figures 1–4). It is straightforward to observe the non-uniformity in the line splittings and intensities. The lowest component of the $^4F_{7/2}$ level with the crystallographic c axis perpendicular to B (figure 1) has shown another type of transition, associated with the splitting of the ground-state doublet of the $^4I_{9/2}$ level. In fact, since the levels are not pure, all transition between crystal-field levels would have to exhibit four split lines. This has

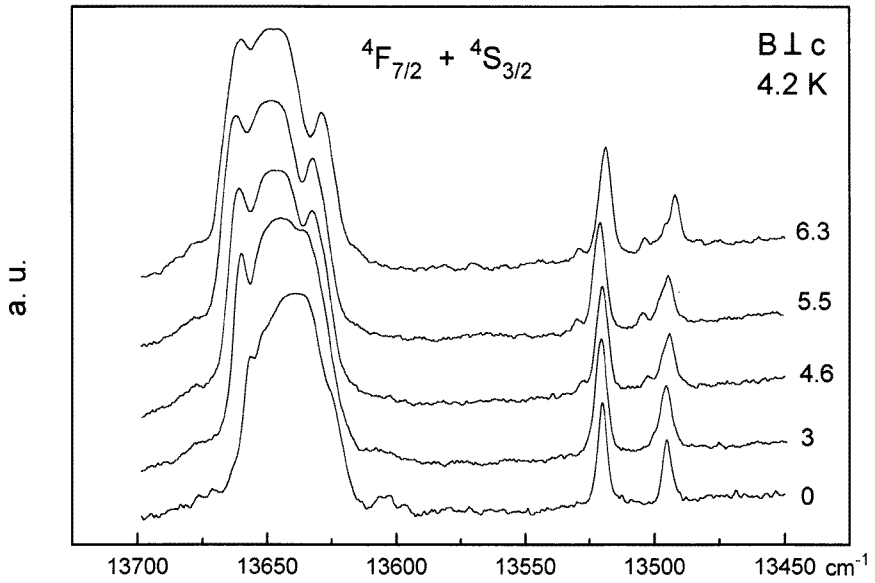

Figure 1. Absorption spectra of the $^4F_{7/2} + {}^4S_{3/2}$ levels with $B \perp c$ (a.u., arbitrary units). The components of the latter are very mixed.

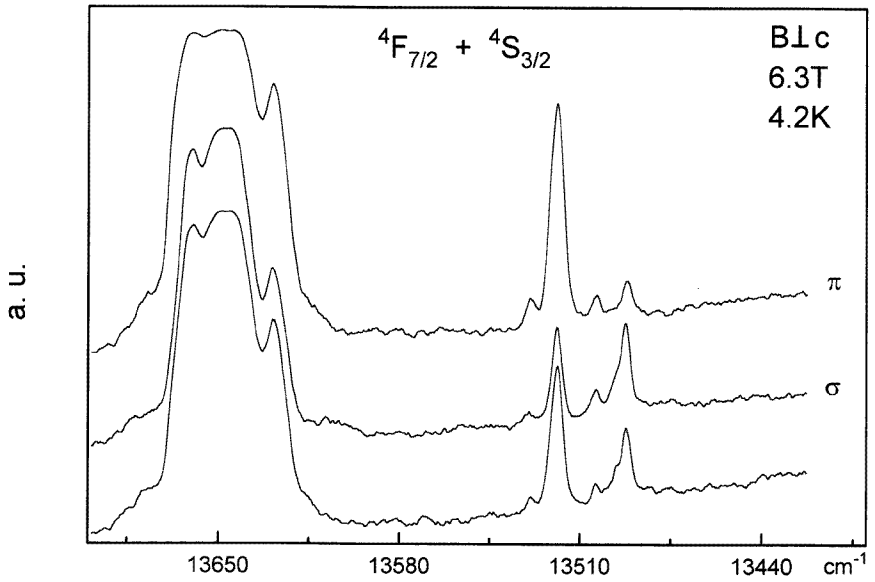

Figure 2. Polarized absorption spectra of the $^4F_{7/2}$ level (a.u., arbitrary units). $B = 6.3$ T perpendicular to c. The transition from the first excited level to the lowest component of this level is observed.

not been observed, partially because the first excited level (arising from the ground-value Kramers doublet splitting) does not have a significant thermal population. The polarized

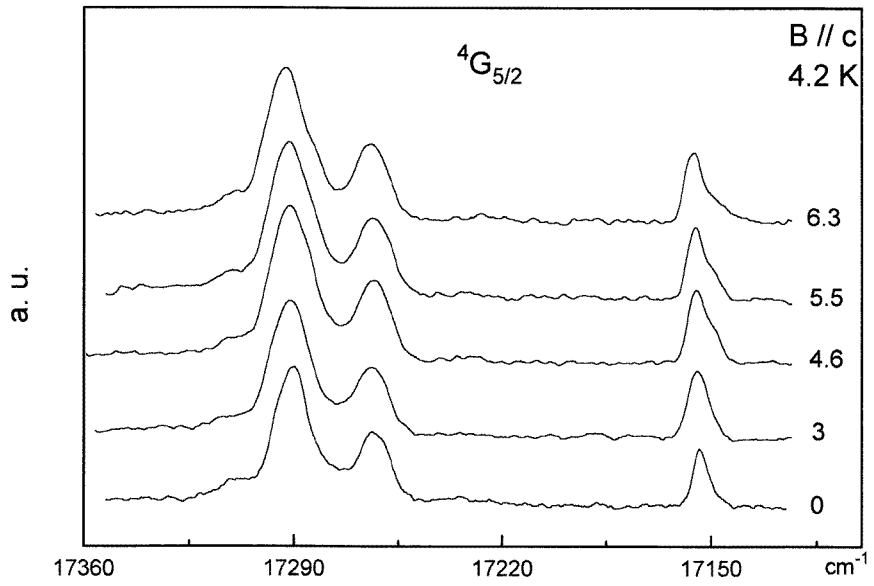

Figure 3. Absorption spectra of the $^4G_{5/2}$ level with $B \parallel c$ (a.u., arbitrary units).

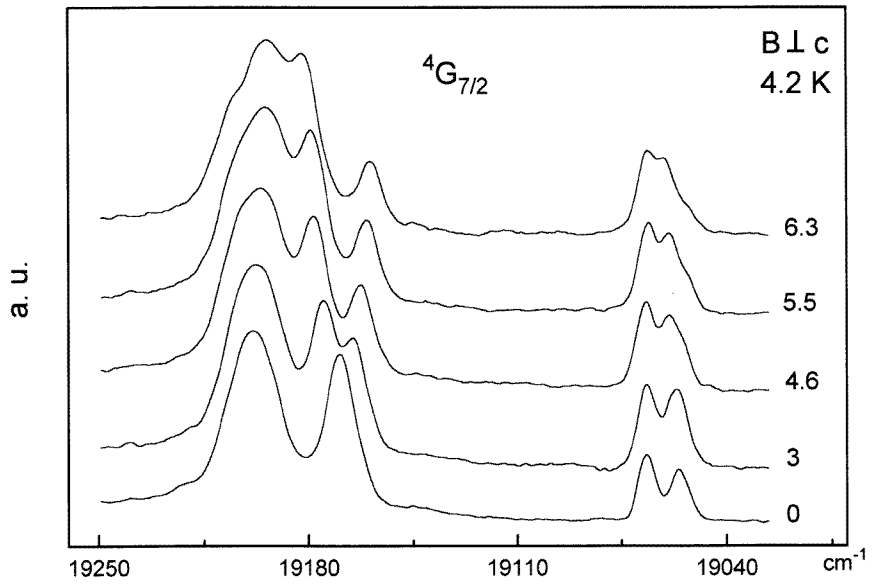

Figure 4. Absorption spectra of the $^4G_{7/2}$ level with $B \perp c$ (a.u., arbitrary units).

spectrum of the $^4F_{7/2}$ level (figure 2) shows that the transition from the first excited level is allowed by σ polarization. However, only one transition of this type has been observed and it was not possible to define the one-dimensional irreducible representation of the split lines. The $^4S_{3/2}$ level has appeared superposed on the two final components of this multiplet

for all orientations of the axis c. This has led to an unresolved Zeeman pattern, and one can only observe the magnetic displacement of the first and the last lines grouped. The $^4F_{9/2}$ level shows a very interesting behaviour under a magnetic field ($B \perp c$). Their four first lines experience a magnetic two-by-two repulsion. This will be exploited later when discussing the magnetic field strength.

The $^4G_{5/2}$ level in figure 3 with $B \parallel c$ constitutes an example where the magnetic field almost does not affect the position of the lines. Figure 4 shows the opposite situation for the $^4G_{7/2}$ level. The third component of this level exhibits a relatively important splitting under the effect of a magnetic field, with a difference in energy of 23 cm^{-1} when $B = 6.3$ T.

In our experiment, no one level in the absorption spectra under a magnetic field has shown a strong displacement of its barycentre. This is an indication that the Kramers degeneracy of the ground-state doublet is only slightly removed.

4.1.1. Simulation of the energy level scheme. The calculations have been performed by programs which are a FORTRAN translation of the Racah algebraic formalism as discussed by Wybourne [26, 27]. A D_{2d} site symmetry is assumed first. In a second step, the imaginary part of the crystal-field parameters, i.e. S_4^k, is introduced to realize the descending $D_{2d} \rightarrow S_4$ site symmetry. The minimizing procedure considers the rms standard deviation σ as a factor of merit:

$$\sigma = \sqrt{\sum (E_{exp} - E_{calc})^2 \Big/ N_\ell - N_p} \tag{13}$$

where E_{exp} are the experimental levels, E_{calc} are the levels from simulation, and N_ℓ and N_p are the number of experimental levels and the number of parameters involved in the simulation, respectively.

The programs calculate the 182 energy positions of the Kramers doublets and compare them with the experiment. The secular determinant is divided into two 91×91 submatrices, corresponding to the two possible crystalline quantum numbers ($\mu = \frac{1}{2}, \frac{3}{2}$) and irreducible representations. All 137 observed levels were introduced in the simulation (table 1). The $^4I_{11/2}$ experimental level was obtained from [3]. For the D_{2d} point symmetry, 19 parameters were used to reproduce the energy level scheme. For S_4 symmetry, an arbitrary choice of the azimuthal angle in spherical coordinates permits us to set S_4^4 equal to zero, but letting the modulus $|B_4^4 + iS_4^4|$ constant. In this way, the only imaginary parameter to consider is S_4^6, i.e. 20 parameters varying freely.

The values of the final sets of parameters deduced from the simulation and their uncertainties are shown in table 2. The starting values are from [7]. The simulation is rapidly achieved and a rms deviation of 17.7 cm^{-1} has been calculated. It is noteworthy that all parameters vary freely. Effectively, the $^2F(2)$ terms observed far in the UV permit us to vary freely T^3 and γ and these parameters are well estimated [6]. The parameters B_0^6 and S_4^6 are found with relatively poor precision in both symmetries, whereas the other parameters are well defined. The simulation performed here appears more complete than the simulation of [9], where 110 energy levels and 27 parameters were considered. The main difference with respect to the present work lies in the introduction of the M^k and P^k free-ion parameters and in the fact that S_4^4 and S_4^6 are varying together freely.

In comparing our result with [10], we see that we have calculated a smaller value of σ with a more complete experimental level scheme. Moreover, the contribution due to the $^2H(2)_{11/2}$ level here is about 11% as against 19% in [10], when considering the five lines measured. This discussion allows us to suggest that complete knowledge of the experimental

Table 1. Experimental and calculated energy levels of the 1% Nd-doped $LiYF_4$ ($T = 9$ K). (From [3].)

	Energy level		
		Calculated	
$^{2S+1}L_J$	Experimental	S_4	D_{2d}
$^4I_{9/2}$	0	8	8
	136	147	147
	179	188	188
	244	252	252
	524	541	541
$^4I^{(1)}_{11/2}$	1997	1990	1990
	2040	2028	2028
	2042	2035	2035
	2077	2065	2065
	2227	2228	2228
	2262	2263	2263
$^4I_{13/2}$	3944	3940	3940
	3958	3966	3966
	3993	3983	3983
	4026	4013	4013
	4206	4208	4208
	4218	4232	4232
	4244	4240	4240
$^4I_{15/2}$	5853	5855	5855
	5914	5914	5914
	5949	5947	5947
	6018	6027	6027
	6318	6318	6318
	6350	6359	6359
	6386	6386	6386
	6436	6437	6433
$^4F_{3/2}$	11 545	11 521	11 521
	11 609	11 568	11 568
$^4F_{5/2} + {}^2H(2)_{9/2}$	12 538	12 518	12 518
	12 547	12 558	12 558
	12 628	12 637	12 637
	12 645	12 658	12 658
	12 666	12 690	12 690
	12 733	12 797	12 797
	12 806	12 815	12 815
		12 891	12 891
$^4F_{7/2} + {}^4S_{3/2}$	13 497	13 502	13 502
	13 522	13 524	13 524
	13 630	13 629	13 629
	13 642	13 634	13 634
	13 656	13 652	13 652
	13 660	13 655	13 655

Table 1. (Continued)

	Energy level		
		Calculated	
$^{2S+1}L_J$	Experimental	S_4	D_{2d}
$^4F_{9/2}$	14 749	14 762	17 762
	14 777	14 786	14 786
	14 877	14 875	14 875
	14 891	14 885	14 885
	14 948	14 945	14 945
$^2H(2)_{11/2}$	15 963	15 988	15 988
	15 990	15 990	15 990
		16 009	16 009
	16 035	16 022	16 022
	16 050	16 050	16 050
	16 134	16 080	16 080
$^4G_{5/2} + {}^2G(1)_{7/2} + {}^4G_{7/2}$	17 156	17 169	17 169
	17 266	17 245	17 245
	17 293	17 296	17 296
	17 405	17 388	17 388
	17 413	17 399	17 399
	17 471	17 464	17 464
	17 645	17 630	17 630
	19 060	19 021	19 021
	19 069	19 069	19 070
	19 173	19 175	19 175
	19 202	19 188	19 188
$^4G_{9/2} + {}^4K_{13/2}$	19 454	19 466	19 466
	19 550	19 552	19 552
	19 601	19 602	19 602
	19 654	19 678	19 678
	19 678	19 690	19 690
	19 709	19 699	19 699
		19 722	19 722
		19 726	19 726
	19 744	19 745	19 745
		19 784	19 784
	19 982	19 980	19 980
	20 005	19 994	19 994
$^2G(1)_{9/2}$	21 041	21 020	21 020
	21 052	21 061	21 061
	21 059	21 090	21 090
	21 087	21 095	21 095
	21 177	21 176	21 176

level scheme can produce a good fitted level scheme, in the case of the Nd^{3+} ion, dealing only with the usual free-ion and crystal-field parameters.

Table 1. (Continued)

	Energy level		
		Calculated	
$^{2S+1}L_J$	Experimental	S_4	D_{2d}
$^2D(1)_{3/2}$	21 272	21 281	21 281
	21 312	21 301	21 301
$^4G_{11/2} + {}^2K_{15/2}$	21 444	21 454	21 454
		21 473	21 473
	21 542	21 568	21 568
	21 702	21 670	21 670
	21 737	21 733	21 734
	21 765	21 762	21 762
		21 775	21 775
		21 796	21 795
	21 804	21 811	21 811
	21 829	21 812	21 812
	21 893	21 899	21 899
	21 936	21 943	21 943
	21 975	21 989	21 989
		22 010	22 010
$^2P_{1/2}$	23 381	23 344	23 344
$^2D(1)_{5/2}$	23 882	23 878	23 878
	23 928	23 919	23 919
	24 025	23 995	23 995
$^2P_{3/2}$	26 254	26 251	26 251
	26 332	26 316	26 316
$^4D_{3/2}$	28 095	28 082	28 082
	28 201	28 197	28 197
$^4D_{5/2}$	28 355	28 356	28 356
	28 510	28 516	28 516
	28 566	28 564	28 564
$^4D_{1/2}$	28 787	28 814	28 814
$^2I_{11/2}$	29 195	20 224	29 224
	29 279	29 307	29 307
	29 364	29 389	29 389
	29 492	29 503	29 503
		29 678	29 678
	29 681	29 687	29 687

4.1.2. Effect of the magnetic field strength. Calculations involving the magnetic field have been performed assuming a D_{2d} point symmetry. Free-ion and crystal-field parameters previously determined are kept constant. The $^4I_{9/2} \rightarrow {}^4F_{7/2} + {}^4S_{3/2}$ and $^4I_{9/2} \rightarrow {}^4F_{9/2}$ transitions are shown in figures 5 and 6 because they can be considered as representative of the general behaviour. The doublets corresponding M_J-values are in table 3. Note that, for

Table 1. (Continued)

	Energy level		
		Calculated	
$^{2S+1}L_J$	Experimental	S_4	D_{2d}
$^2L_{15/2} + {}^4D_{7/2} + {}^2I_{13/2}$	30 222	30 217	30 217
	30 280	30 267	30 268
		30 322	30 322
	30 359	30 346	30 346
	30 432	30 413	30 413
		30 452	30 452
		30 463	30 463
	30 492	30 473	30 473
		30 535	30 535
	30 568	30 587	30 587
	30 665	30 670	30 670
		30 675	30 675
		30 702	30 702
	30 750	30 741	30 742
		30 766	30 766
		30 898	30 898
	30 922	30 931	30 931
	31 022	31 036	31 036
		31 045	31 045
$^2L_{17/2}$		31 719	31 719
	31 797	31 795	31 795
	31 858	31 851	31 851
	31 935	31 931	31 931
		31 969	31 969
		32 019	32 019
	32 078	32 034	32 034
		32 164	32 164
		32 176	32 176
$^2H(1)_{9/2}$	32 927	32 940	32 940
	33 020	33 031	33 031
		33 045	33 045
	33 097	33 103	33 103
		33 144	33 144
$^2D(2)_{3/2}$	33 434	33 472	33 472
		33 557	33 557

an easier comprehension of these figures, the experimental levels are supposed to coincide with the calculated levels in the absence of a magnetic field (which is not true for the energy level simulation in table 1). From the measured splitting versus magnetic field, we can make four remarks.

(i) Experimentally, for the range of magnetic fields that we have worked with, linear as well as non-linear anticrossing degeneracy lifting has been observed (e.g. figure 6).

(ii) The simulation of the split doublets is strongly dependent on the levels considered. For the $^4I_{9/2} \rightarrow {}^4G_{7/2}$ and $^4I_{9/2} \rightarrow {}^4G_{5/2}$ transitions the simulation is rather good when B

Table 1. (Continued)

	Energy level		
		Calculated	
$^{2S+1}L_J$	Experimental	S_4	D_{2d}
$^2H(1)_{11/2} + {}^2D(2)_{5/2}$	34 235	34 247	34 247
	34 301	34 316	34 316
		34 346	34 346
		34 436	33 436
		34 439	34 439
	34 490	34 510	34 510
	34 530	34 534	34 534
	34 654	34 654	34 654
		34 663	34 663
$^2F(2)_{5/2}$		38 555	38 555
	38 679	38 653	38 653
	38 710	38 732	38 732
$^2F(2)_{7/2}$		39 937	39 937
	39 973	39 958	39 958
	40 024	40 020	40 020
	40 095	40 116	40 116
$^2G(2)_{9/2}$		47 632	47 632
		47 729	47 729
	47 740	47 737	47 737
		47 824	47 824
	47 847	47 852	47 852
$^2G(2)_{7/2}$	48 506	48 495	48 495
	48 596	48 572	48 571
		48 690	48 690
		48 758	48 758
$^2F(1)_{7/2}$		65 933	65 933
		66 201	66 201
		66 378	66 378
		66 435	66 435
$^2F(1)_{5/2}$		67 223	67 223
		67 570	67 570
		67 642	67 642

is parallel to c (not shown); on the contrary, when B is perpendicular to c, for the same transitions, the simulation is rather poor (not shown). Both cases have linear splitting. This is evidenced by the s_i-values in table 3. This has been previously observed in NdOCl [28]. In the absence of B, the contribution of the level $^4G_{5/2}$ to σ is 1.72%, which means that it is satisfactorily simulated. After turning B on, the simulation is no longer good. The origin of such discrepancy is not clear but is quantitatively due to the ket composition in the wavefunctions associated with each quantum state.

(iii) For the $^4I_{9/2} \rightarrow {}^4F_{7/2} + {}^4S_{3/2}$ (figure 5) and $^4I_{9/2} \rightarrow {}^4F_{9/2}$ (figure 6) transitions

Table 2. Final values of the parameters used in the simulation for both D_{2d} and S_4 symmetries.

	Value (cm^{-1})		
Parameter	D_{2d}	S_4	Uncertainty
E^0	23 726	23 726	1
E^1	4821.7	4821.7	0.7
E^2	23.72	23.72	0.01
E^3	485.37	485.57	0.07
α	21.79	21.79	0.03
β	−604	−604	3
γ	1513	1513	4
T^2	365	365	2
T^3	41	41	2
T^4	86	86	2
T^6	−251	−251	5
T^7	321	321	5
T^8	373	373	6
ξ	874.5	874.5	0.6
B_0^2	421	421	10
B_0^4	−985	−985	27
B_4^4	−1146	−1146	17
S_4^4	—	0.0	—
B_0^6	7	7	27
B_4^6	−1074	−1073	16
S_4^6	—	38	333
$\sum(E_{exp} - E_{sim})^2$	36 791	36 789	—
σ	17.7	17.7	—

the splitting is not linear. In particular, the second transition presented an anticrossing behaviour. Indeed, there is no completely linear splitting. This is a phenomenological demonstration that the wavefunctions are non-degenerate.

These last two features can *only* be simultaneously reproduced if the Zeeman operator is introduced in the secular determinant *before* diagonalization, because in this way the magnetic strength effects are taken into account all together.

(iv) One can see that the experimental and simulated splitting factors of the ground doublet are close to each other (table 3). In figure 1, the position of the lowest peak essentially does not change with increasing magnetic field. This corroborates the assertion that the ground state splits only slightly.

5. Conclusion

The simulation of the Nd^{3+}-doped $LiYF_4$ energy level scheme has been re-examined with an increased number of experimental levels (137). The approximate D_{2d} site symmetry as well as the real S_4 symmetry were considered. A better phenomenological set of free-ion and crystal-field parameters has been found, as indicated by a smaller value of the rms deviation when compared with previous results [10]. This leads to the supposition that, in the case of the Nd^{3+} ion, a more complete experimental level scheme will lead to a more adequate set of free-ion and crystal-field parameters, and then to produce a better calculated level scheme,

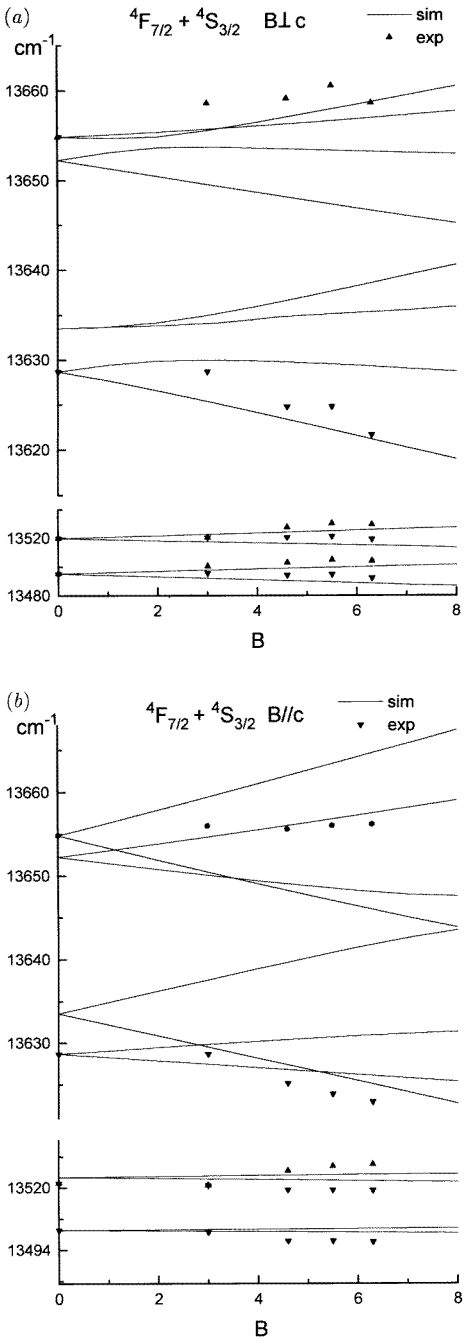

Figure 5. Simulation and experimental energies of the $^4F_{7/2}$ and $^4S_{3/2}$ levels with (*a*) $B \perp c$ and (*b*) $B \parallel c$: ● , no observed splitting.

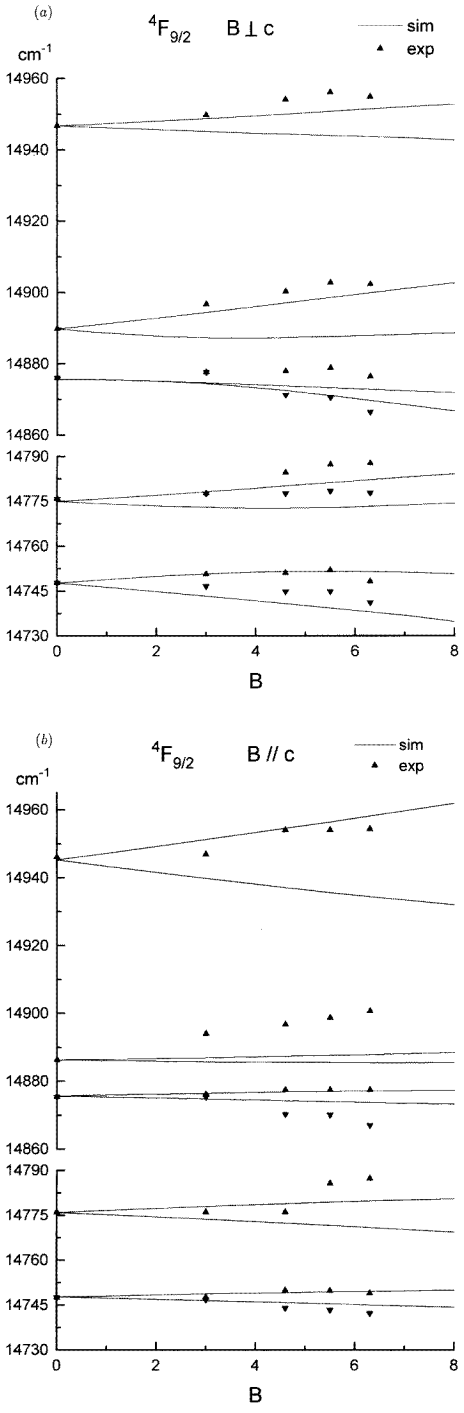

Figure 6. Simulation and experimental results of the $^4F_{9/2}$ level with (*a*) $B \perp c$ and (*b*) $B \parallel c$.

Table 3. Experimental and simulated values of the splitting factors $s_{\parallel}$ and $s_{\perp}$. The values of M_J have been obtained from the more important simulated component.

		$s_{\parallel}$		$s_{\perp}$	
Level	M_J	Experimental	Calculated	Experimental	Calculated
$^4I_{9/2}$	9/2	—	0.69	0.95	1.18
$^4F_{7/2} + {}^4S_{3/2}$	1/2	—	0.16	1.84	1.90
	3/2	1.75	0.30	1.60	1.69
	1/2	—	—	—	—
	3/2	—	—	—	—
	5/2	—	—	—	—
	7/2	—	—	—	—
$^4F_{9/2}$	1/2	—	0.69	—	—
	3/2	—	1.39	—	—
	5/2	—	0.50	—	—
	7/2	—	0.36	—	—
	9/2	—	3.75	2.5	1.26
$^4G_{5/2}$	3/2	—	0.31	1.35	0.32
	1/2	0.00	0.15	—	0.66
	5/2	0.77	1.04	1.63	0.20
$^4G_{7/2}$	1/2	—	0.00	1.29	1.44
	3/2	1.46	1.36	0.00	0.31
	5/2	1.61	1.77	3.43	0.21
	7/2	1.80	1.84	1.62	0.20

with no need for further parameters. The absorption spectra of the Nd^{3+} ions under a magnetic field have emphasized the experimental difficulties in measuring the line splitting, as already reported [17]. For the isolated doublets, the calculation gives $s_{\perp}$- and $s_{\parallel}$-values in good agreement with experiment, except for a few cases. For most levels in the visible it was shown that the Zeeman effect is of a non-linear anticrossing nature with respect to B. The *only* way of obtaining the linear and non-linear behaviours of the split states versus magnetic field is through introducing the magnetic operator in the secular determinant *before diagonalizing it*. The differences between the phenomenological simulation and experience indicate that the components of the eigenfunctions expansion representing the crystal-field levels still play a crucial role. However, in some cases the discrepancy is so important that it is probably necessary to introduce another type of interaction or to complete the energy level scheme.

Acknowledgments

One of the authors (MACS) wish to acknowledge the CNPq (Brazilian agency) and CNRS (French agency) for financial support, Dr E Antic-Fidancev, Mrs M Lemaître-Blaise and Mrs J Derouet are also gratefully acknowledged for technical help and fruitful discussions.

References

[1] Ramaz F, Vial J C and Macfarlane R M 1992 *J. Lumin.* **53** 244
[2] Taibi M, Antic-Fidancev E, Aride J, Lemaître-Blaise M and Porcher P 1993 *J. Phys.: Condens. Matter* **5** 5201
[3] Anderson F G, Weidner H, Summers P L and Peale R E 1994 *J. Lumin.* **62** 77
[4] Godlewski M and Leskelä M 1994 *Crit. Rev. Solid State Mater. Sci.* **19** 1994
[5] Xu W, Chen G and Peterson J R 1995 *J. Solid State Chem.* **115** 71
[6] Morrison C A and Wortman D E June 1995 *Army Research Laboratory Technical Report* ARL-TR-635
[7] da Gama A A S, de Sá G F, Porcher P and Caro P 1981 *J. Phys. Chem. Solids* **75** 2583
[8] Wortman D E, Karayianis N and Morrison C A August 1976 *Harry Diamond Laboratories Technical Report* HDL-TR-1770 (*National Technical Information Services Report* NTIS AD A033 902)
[9] De Leebeeck H and Görller-Walrand C 1995 *J. Alloys Compounds* **225** 75–9
[10] Görller-Walrand C, Fluyt L, Porcher P, da Gama A A S, de Sá G F, Carnall W T and Goodman G L 1989 *J. Less-Common Met.* **148** 339
[11] Dieke G H and Heroux L 1955 *Phys. Rev.* **130** 1227
[12] Guillot M, Marchand A, Nekvasil V and Tcheou F 1985 *J. Phys. C: Solid State Phys.* **18** 3547
[13] Pilawa B 1990 *J. Phys.: Condens. Matter* **2** 5555
[14] Pourat B, Pilawa B and Kahle H G 1991 *J. Phys.: Condens. Matter* **3** 6069
[15] Koster G F and Statz H 1958 *Phys. Rev.* **113** 445
[16] Statz H and Koster G F 1958 *Phys. Rev.* **115** 1568
[17] Hayhurst T, Shalimoff G, Conway J G, Edelstein N, Boatner L A and Abraham M M 1982 *J. Chem. Phys.* **76** 3960
[18] Görller-Walrand C, Behets M, Porcher P and Laursen I 1982 *J. Chem. Phys.* **83** 4329
[19] Enderle M, Pilawa B and Kahle H G 1990 *J. Phys.: Condens. Matter* **2** 4711
[20] Lerner R G and Trigg G L 1990 *Encyclopedia of Physics* (New York: VCH)
[21] Carnall W T, Goodman G L, Rajnak K and Rana R S 1988 *Argonne National Laboratory Report*
[22] Beaury L, Derouet J, Escorne M and Porcher P 1994 *J. Phys.: Condens. Matter* **6** 5169
[23] Porcher P 1978 *PhD Thesis* Université Paris VI
[24] Judd B R 1962 *Phys. Rev.* **127** 750
[25] Caro P 1976 *Structure Électronique des Éléments de Transition: l'Atome dans le Cristal* 1st edn (Paris: Presses Universitaires de France)
[26] Porcher P 1989 *FORTRAN programs REEL and IMAGE for Simulation of the d^N and f^N Configurations involving Real and Complex Crystal Field Parameters, as well as Magnetic Field* unpublished
[27] Wybourne B G 1965 *Spectroscopic Properties of Rare Earths* (New York: Wiley)
[28] Beaury L, Derouet J, Porcher P, Caro P and Feldman P G 1986 *J. Less-Common Met.* **126** 263